

Reconnection scaling experiment: A new device for three-dimensional magnetic reconnection studies

I. Furno,^{a)} T. Intrator, E. Torbert, C. Carey, M. D. Cash, J. K. Campbell, W. J. Fienup, C. A. Werley, and G. A. Wurden
Los Alamos National Laboratory, Mail Stop E526, Los Alamos, New Mexico 87545

G. Fiksel

Department of Physics, University of Wisconsin–Madison, 1150 University Avenue, Madison, Wisconsin 53706

(Received 14 October 2002; accepted 18 November 2002)

The reconnection scaling experiment (RSX), a linear device for studying three-dimensional magnetic reconnection in both collisional and collisionless laboratory plasmas, has been constructed at Los Alamos National Laboratory. Advanced experimental features of the RSX that lead to scientific advantages include the use of simple technology (commercial plasma guns) to create plasma and current channels. Physics motivations, design and construction features of the RSX, are presented. Basic plasma parameters that characterize the RSX are shown together with preliminary measurements of visible light emission during the merging of two parallel current channels.

© 2003 American Institute of Physics. [DOI: 10.1063/1.1544051]

I. INTRODUCTION AND THEORETICAL BACKGROUND

Magnetic reconnection refers to the local breaking of magnetic field lines and subsequent change in the global topology of the magnetic field^{1,2} in the presence of plasmas or conducting fluids. During this process, magnetic field lines of opposite polarity are convected toward each other by fluid flow in the so-called diffusion region. In this region, the “frozen-in” condition of ideal magnetohydrodynamics (MHD) equations is broken. The magnetic field can diffuse through the plasma, allowing the annihilation of opposite directed magnetic field lines and the conversion of magnetic energy into ohmic heating and particle acceleration. Magnetic reconnection in plasmas is considered to play a crucial role in a variety of different astrophysical and laboratory phenomena. Some examples are in the evolution of solar flares,^{3,4} in the dynamics of the Earth magnetosphere,^{5–7} and in the redistribution of the energy in the universe.⁸ In magnetically confined laboratory plasmas for fusion research, a major role is played by magnetic reconnection in determining the dynamics of relaxation processes, such as sawtooth oscillations in tokamaks⁹ and dynamo effects in reversed field pinches.¹⁰

During the last decades, the theory of magnetic reconnection in two dimensions (2D) has been highly developed and is now fairly well understood. Early attempts to explain 2D magnetic reconnection were based on resistive MHD equations, in which finite plasma resistivity η in Ohm's law is responsible for the breakdown of the frozen-in condition in the diffusion region. Within this framework, Sweet and Parker (SP)^{11–14} developed a steady state model in which the characteristic time scale of the reconnection process is $\tau_{SP} = S^{1/2}\tau_A$, where τ_A is the Alfvén time and S is the Lundquist

number. Although the Sweet–Parker model provides a qualitative picture of the reconnection process, the predicted reconnection rates are orders of magnitude too small to account for space physics observations such as solar flares where $S \sim 10^{12} - 10^{14}$. Recently, several theoretical and numerical studies suggested that a more complete description of reconnection requires the adoption of a generalized Ohm's law which takes into account the electron dynamics. Simulations of reconnections in a 2D system from Hall MHD, hybrid and full particle-in-cell codes^{15–17} showed that electron dynamics enable much faster reconnection than resistive MHD. Details of the electron dynamics are not important for the global reconnection rate, which is still determined in a 2D system by the ion dynamics.

The complexity of the magnetic reconnection process is further compounded by intrinsic three-dimensional (3D) features of space and astrophysical plasmas. The development of a wide variety of kinetic instabilities could significantly alter the reconnection rate, the structure of the dissipation region, and the release of magnetic energy. Simulations in full 3D configurations^{18,19} are in early stages and there is not yet concurrence concerning the physics.

Aside from plasma magnetic fusion experiments, Earth based and space satellite observations, a number of existing experiments are (or were) dedicated to investigations of the physics of magnetic reconnection. Early linear experiments used fast high density pinch devices and their data were analyzed in the context of MHD physics.^{20–24} Following experiments in the Large Plasma device (LPD)^{25–31} provided detailed measurements of the relaxation to a force-free state produced by the coalescence of two current channels. Interacting current channels were produced by coating a large cathode source nonuniformly and then biasing it with respect to an external anode. Although 3D features of magnetic reconnection were studied in the electron MHD (EMHD) re-

^{a)}Electronic mail: furno@lanl.gov

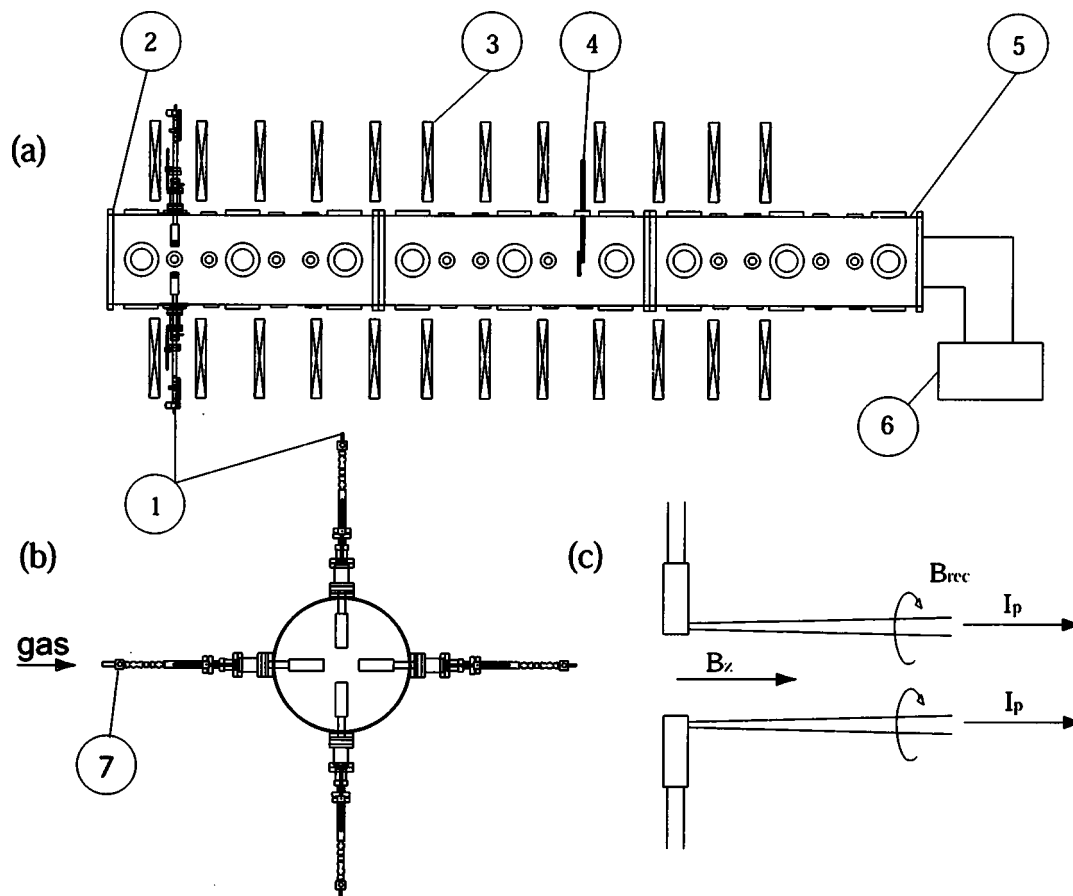


FIG. 1. Cross section of the RSX device: (a) lateral view, (b) front view, and (c) schematics of two current channels interacting along the axis of the device. The RSX main elements shown are (1) plasma guns, (2) head flange that accommodates a large window, (3) magnet coils, (4) external anode, (5) stainless steel vacuum vessel, (6) schematics of the vacuum system, and (7) electromechanical valve for gas puffing.

gime (electrons are magnetized but ions are not), the Lundquist number ($S \leq 10$) of the interacting current channels was limited by the plasma production scheme. The next generation of experiments with large Lundquist number are carried out by axially merging two toroidal spheromak-like plasmas in Tokyo University Spherical Torus No. 3³²⁻³⁴ and merging two toroidal plasmas in the Magnetic Reconnection Experiment^{35,36} and the Swarthmore Spheromak Experiment.³⁷⁻⁴⁰ A recent toroidal and collisionless experiment takes advantage of cusp geometry.⁴¹

The challenging physics of 3D magnetic reconnection and the large number of open questions motivated a new experimental investigation of reconnection in high S plasmas with a focus on three-dimensional issues.

Over the past few years, developments in plasma gun technology have made plasma guns a reliable laboratory source capable of producing plasmas with large Lundquist numbers ($S \approx 800$).^{42,43} The reconnection scaling experiment (RSX) at Los Alamos National Laboratory will use this innovative plasma gun technology to create parallel current channels and to study their coalescence in 3D linear geometry. The emphasis will be on using many repetitive plasma discharges to acquire detailed spatial and temporal measurements as the two current channels merge along the axis of the linear device.

The rest of the article is organized as follows: in Sec. II,

the design and construction of the RSX is reviewed together with the plasma gun technology and details of machine operation. In Sec. III, preliminary measurements of RSX plasmas are presented and discussion is outlined in Sec. IV.

II. RSX EXPERIMENTAL APPARATUS

A view of the RSX device is shown in Figs. 1(a) and 1(b) together with a schematic of the linear geometry of two interacting current channels, Fig. 1(c). Here in Sec. II, the main elements of the RSX device are described together with the plasma production technique. An overview is presented of the control and data acquisition system and main diagnostics.

A. Vacuum vessel and vacuum system

The RSX vessel consists of a cylindrical vacuum chamber of approximately 4 m length and 20 cm radius, Fig. 1(a), which is formed by three sections 48 in. in length recycled from the field reversed configuration experiment (FRX-C)⁴⁴ and fabricated from stainless steel (SS304) tubing with a 40.6 cm nominal outside diameter and a 0.48 cm wall thickness. Each section has 16×2.75 and 12×6 in. Conflat flanges facing radially, allowing easy placement of the diagnostics and flexibility in the plasma gun geometry arrangement. End flanges accommodate large windows, probe access, and

eventually mounts for plasma gun arrays. The use of standard Conflat hardware ensures ultrahigh vacuum capability at reasonable cost. The vacuum system consists of a 5500 l/s roughing and backing mechanical pumps with a 110 l/s turbopump which provides a 10^{-7} Torr base vacuum before plasma formation. The vacuum control system encompasses an automatic gauge controller and safety interlock which closes appropriate valves and shuts down the turbopump in the case of accidental pressure or power failure. During operation of the plasma guns, this system is disabled to prevent its intervention following plasma formation and the subsequent increase in pressure.

B. Plasma guns, pulser supply, and discharge sequence

Presently, RSX is equipped with four plasma guns radially inserted through 2.75 in. flanges into the vacuum chamber and equally spaced in the poloidal direction as shown in Fig. 1(b). The plasma guns, originally designed^{42,43} for current profile modification in the Madison symmetric torus,⁴⁵ allow the injection of parallel current channels along the axial direction of the RSX device as is schematically shown in Fig. 1(c). The radial distance between plasma guns can be modified to provide flexibility in the geometry of the interacting current channels.

Each plasma gun, with a 5 cm external diameter, contains a miniaturized plasma source with a circular 0.79 cm² nozzle aperture in which a cylindrical plasma is produced by arc discharge between a molybdenum anode and a cathode.⁴³ A stack of molybdenum and boron nitride washers 1.5 cm high defines the arc channel between the anode and the cathode. The gas, usually H or He, is supplied through the cathode by an electromagnetic valve, Fig. 1(b), which is pulsed 12 ms before arc discharge. This time delay corresponds to the gas traveling time from the puff valve to the miniaturized discharge chamber. When the arc anode is negatively biased with respect to an external anode, a fraction of the arc current is diverted towards the external anode as plasma current. In Fig. 1(a), the external anode is shown that consists of a 50 cm² SS304 plate bolted to a copper rod which is electrically insulated from the vacuum vessel by a ceramic feedthrough. The external anode can be moved along the RSX vessel to modify the length of a single current channel.

In Fig. 2, a schematic of the discharge pulser circuit is shown. The arc plasma is maintained by a pulse forming network (PFN) which sets the internal gun arc voltage to $V_{\text{arc}} = 80\text{--}100$ V and determines the discharge pulse length which is presently approximately 10 ms. The impedance of the PFN matches the arc impedance and is set to 100 m Ω . The PFN capacitors are charged up to a maximum voltage $V_{\text{cap}} = 1$ kV and the arc discharge is initiated by applying a gate pulse to a silicon controlled rectifier (SCR), SCR1 in Fig. 2. The arc current, I_{arc} can be varied from 0.3 to 1 kA. The bias pulser, shown on the left in Fig. 2, is designed to lower the potential of the arc anode below that of the grounded external anode so that, by varying the external bias voltage, $V_{\text{bias}} = 0\text{--}300$ V, a desired fraction of the arc current can be extracted as external anode (i.e., plasma) current. The

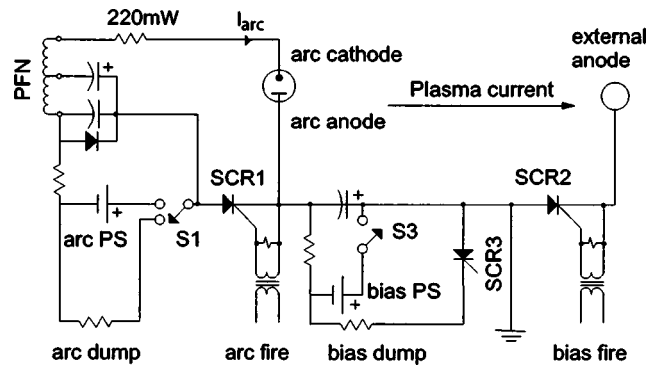


FIG. 2. Schematic of the exciter circuit for the plasma guns. When the arc anode is negatively biased with respect to the external anode, Fig. 1(a), a fraction of the arc current I_{arc} is diverted towards the external anode as plasma current. Shown are the pulse forming network (PFN), the silicon controlled rectifier (SCR), the arc, and bias power supply (PS) with switch relays (S1 and S3).

bias discharge is initiated by applying a gate pulse to SCR2 approximately 1 ms after the beginning of the arc discharge corresponding to the maximum of I_{arc} . The duration of the bias discharge can be manually varied from a few μs to approximately 8 ms by shorting the bias capacitor bank into a dump resistor through SCR3.

An illustration of a RSX discharge sequence is presented in Fig. 3, showing measurements obtained from a single gun. The plasma discharge is initiated at $t = 0$ when the arc anode is biased to $V_{\text{arc}} \approx +100$ V with respect to the arc cathode. The arc current, I_{arc} , rapidly increases and reaches a maximum value of about 1 kA just before the external anode is biased to $V_{\text{bias}} \approx 200$ V at $t = 1$ ms. The rise time of the arc current, approximately $t = 1$ ms, is limited mostly by the pulse forming network. For $1 \leq t \leq 10$ ms, a current channel is formed and a total current of about 450 A is driven, as indicated by the current collected by the external anode. The rise time of the bias current is of the order of 50 μs . At $t = 10$ ms, the external anode is floated with respect to the plasma gun and therefore no plasma current is driven.

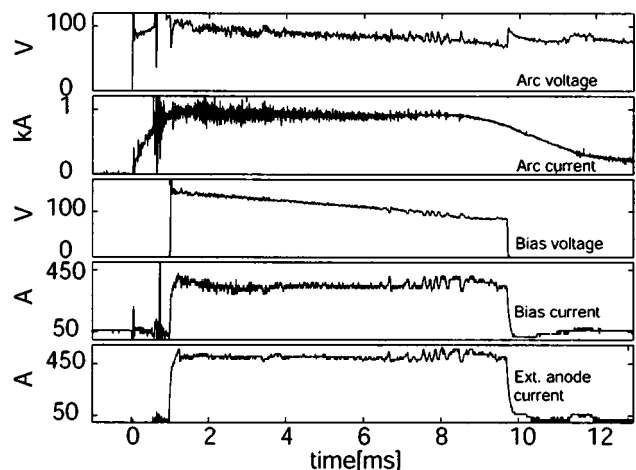


FIG. 3. RSX discharge sequence showing data from a single plasma gun. The time evolution of the arc/bias voltage and current is shown together with the current collected by the external anode.

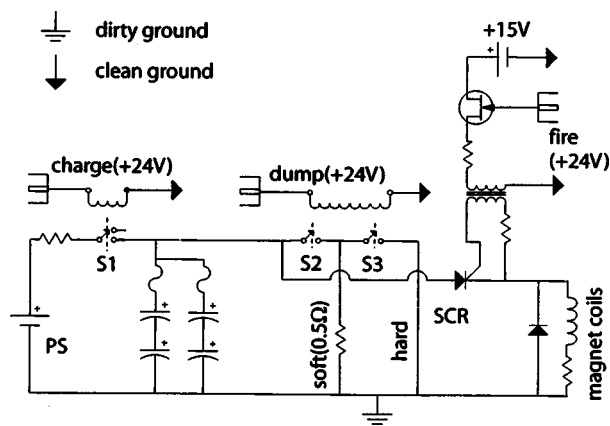


FIG. 4. Schematic of the exciter circuit for the magnet coils together with the MOSFET driver for the SCR switch that starts the discharge. Also shown are the capacitor bank, power supply, and safety circuitry that encompasses two high power switches (S1 and S2) to dump the capacitor bank before and after each discharge.

C. Magnet coils and switching circuit

Figure 4 presents a schematic of the pulse exciter and basic control circuitry for the magnet coils. A set of 12 identical copper coils with 125 cm external diameter and 53 cm internal diameter surrounds the RSX vessel and provides the axial guide field B_z , Fig. 1(a). Each coil has self-inductance of 820 μH and resistance of 80 m Ω . In the present arrangement, a limited set of five pairs of series coils is connected in parallel and energized by an 0.16 F, electrolytic capacitor bank with a quarter cycle time of 16 ms. The capacitor bank is charged by a 800 V, 10 A power supply. For the present capacitor bank and magnet configuration, the maximum center magnetic field is $B_z = 1000$ G at 1 kA current per coil. At this current level, magnet operation only requires a straightforward SCR switched network for a 32 ms half cycle pulse length, with a diode crowbar at the zero voltage crossing time. The SCR is controlled by a metal-oxide-semiconductor field-effect transistor (MOSFET) switch (see Fig. 4) which is gated by a +24 V, 35 ms pulse provided by the control system described in Sec. II E. The power supply control system encompasses automatic safety circuitry (see high voltage switches S2 and S3 in Fig. 4) that shorts the positive and negative sides of the capacitor bank before and after each shot to prevent accidental charging of the capacitor bank. Initial operation at a pulse repetition of 120–180 s can be achieved by air cooling the coils. Water cooling at 10 gal/min using a closed loop de-ionized water system can be easily added to extend operation of the device to a higher repetition rate.

D. Diagnostics

The RSX is equipped with an initial set of diagnostics consisting of internal probes and noninvasive optical systems. Presently, internal probes are inserted into the vacuum vessel through flexible bellows and sliding seals, allowing two-dimensional scanning of plasma parameters in the plane perpendicular to the axis of the device. Each probe can be moved along the axis of the device into a different porthole.

The three components of the magnetic field are measured using a single probe consisting of electrostatically shielded, small (3.175 mm diam), orthogonal magnetic loops with 30 turns each. A miniaturized Rogowski coil⁴⁶ with 1 cm internal diameter allows measurement of the radial profile of current channels. A double Langmuir probe consisting of two electrically insulated tungsten wires enables measurement of the electron density and temperature. A CCD fast framing camera⁴⁷ and multiple photomultiplier tubes allow monitoring of visible light emission from the plasma through portholes.

A feature of paramount importance in 3D magnetic reconnection experiments is the capability to measure plasma parameters and magnetic field structures and fluctuations in three dimensions.⁴⁸ A new three axis moveable probe drive, which will be the subject of a future article, has been designed and is presently under construction. This system will allow a complete three-dimensional scan of the plasma with an interchangeable probe head which accommodates different types of probes.

E. Control and data acquisition system

The RSX control, data acquisition, and data storage system is based on a distributed architecture including a National Instruments FP-2000 Ethernet module and commercial personal computers (PCs). All the machines communicate through Ethernet links.

The FP-2000 module runs embedded LabView Real Time and controls a National Instruments FP-DO-401 discrete output module. This module provides +24 V pulses for the timing sequence with time accuracy within a few ms. Events which require higher accuracy (i.e., gun arc and bias start and stop) are provided by digital hardware delays.

The RSX data acquisition system consists of digital Tektronix oscilloscopes and multiple Le Croy transient recorders which are housed in CAMAC crates controlled via general purpose interface bus (GPIB) interfaces by a commercial PC running Windows 2000. The sequence of configuring and arming the digitizers followed by data retrieval is performed by Labview 6 routines which are grouped into a single graphical user interface. A high level programming language such as Labview 6 allows the use and integration of many different digitizers with only modest software development.

The PC which controls the acquisition system is linked via Ethernet to the RSX data storage system. This consists of a commercial PC running Linux RedHat 7.1 operating system in which a MDS+ server database⁴⁹ is installed. The data are archived on a 60 GB disk drive in MDS+ compressed format and analyzed via Matlab and IDL routines, which allow compatibility with multiple operating systems.

III. INITIAL EXPERIMENTAL DATA

To characterize the flexibility of the RSX, preliminary data are shown for different values of key operating parameters including current density J , electron density n_e , and axial guide magnetic field B_z .

Precise time resolved 3D measurements of particle and field dynamics can be built up over many shots if high re-

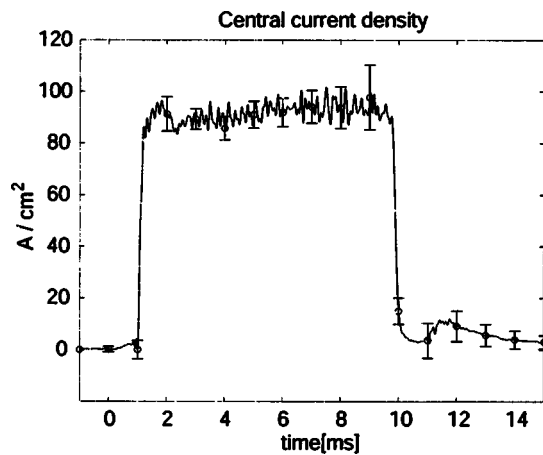


FIG. 5. Time evolution of the center current density measured by a miniaturized Rogowski coil located 100 cm from the gun nozzle. The error bars are calculated from standard deviation of the data over a set of 10 consecutive identical discharges.

producibility of the plasma conditions is provided. The stability of a single plasma gun together with the reproducibility of key plasma parameters has been tested for a set of 10 consecutive discharges over a 30 min period with basic parameters of $V_{\text{arc}}=120$ V, $I_{\text{arc}}=1$ kA, $V_{\text{bias}}=200$ V, $B_z=400$ G, and $P_{\text{gas}}=20$ psi. The center plasma current density was monitored by a miniaturized Rogowski probe.⁴⁶ The gun nozzle and the probe were located at, respectively, $z=0$ and $z=100$ cm. Data were acquired for an approximately 16 ms duration including a 8 ms time window when the external bias was switched on. In Fig. 5, the temporal evolution of the center current density, J_0 , averaged over the complete set of discharges is shown. The error bars are calculated using standard deviation of the data and indicate nominal reproducibility of approximately 7%. In Fig. 5, only a subset of the error bars is shown for clarity. These data demonstrate a major advantage of plasma gun technology, i.e., that many highly reproducible discharges are possible.

Radial profiles of the current density were measured at the same axial location in a set of discharges with basic parameters of $V_{\text{arc}}=100$ V, $I_{\text{arc}}=0.8$ kA, $B_z=400$ G, and $P_{\text{gas}}=35$ psi. In Fig. 6, current density profiles are shown as a function of the external voltage V_{bias} applied as it varies from 0 to 200 V. The total plasma current flowing through the 1 cm² Rogowski aperture was unfolded into a current density profile given by the analytical expression

$$J(r) = \frac{J_0 r_0^2}{r^2 + r_0^2}. \quad (1)$$

Parameters J_0 and r_0 (listed in the inset in Fig. 6) were determined by a least-square fit of the measured total current and the total current calculated from Eq. (1). With this ansatz, changes in radial widths of several millimeters can be resolved. A smaller Rogowski aperture would have better spatial resolution but also a smaller signal to noise ratio.

Figure 6 shows the possibility of varying the ratio between the reconnecting magnetic field, produced by the current channel, and guide field B_z which is an important issue in 3D magnetic reconnection.^{50,51} The maximum current

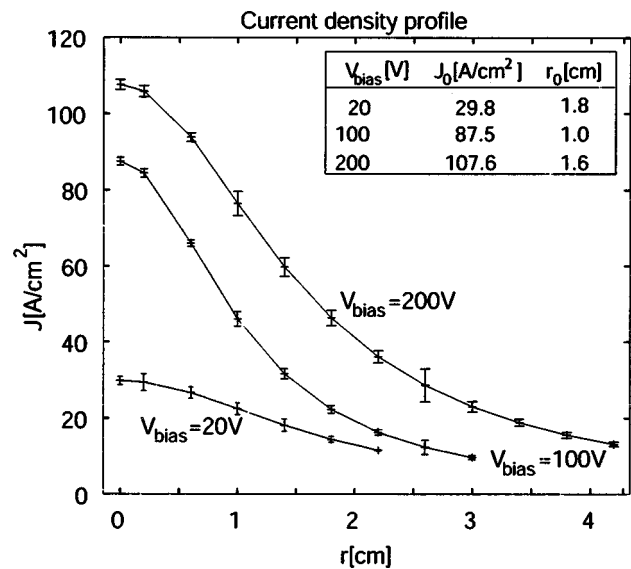


FIG. 6. Current density profiles for different bias voltages. Data were taken with a miniaturized Rogowski coil placed 100 cm from the gun nozzle. The error bars are calculated as standard deviation of the data over a set of three identical discharges. The inset displays profile parameters calculated according to Eq. (1).

density is limited to 100% of the net charge neutral current density. There are overlapping ranges for $J(r)$ profiles that can also be investigated while scanning other parameters such as the magnetic guide field.

For the same set of discharges, Fig. 7 shows the electron density profile before the external bias is switched on. The profile is derived from double electrostatic probe measurements and indicate a center electron temperature of $T_{e0} \approx 10$ eV and center electron density of $n_{e0} \approx 3 \times 10^{13}$ cm⁻³. The shape has a half width half maximum (HWHM) of approximately 2 cm which is only slightly larger than the HWHM of approximately 1.5 cm for the current density data. The plasma density is controlled by the gas plenum pressure, P_{gas} , inside the gun prior to the arc discharge.⁴²

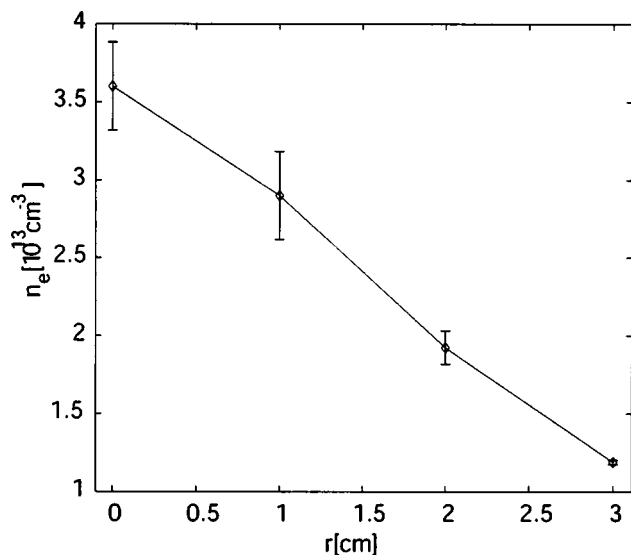


FIG. 7. Electron density profile for $V_{\text{bias}}=0$. Data were taken with a double electrostatic probe placed 100 cm from the gun nozzle.

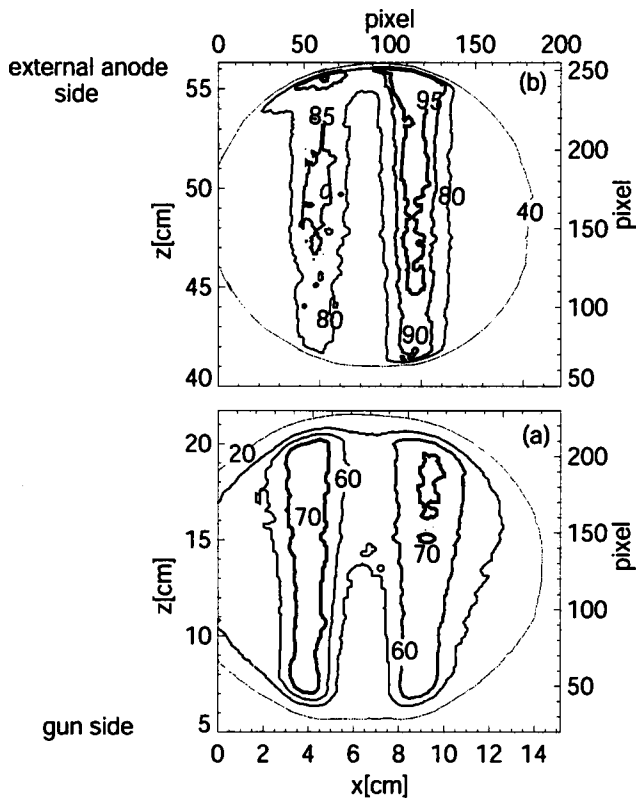


FIG. 8. Visible light emission measured by a Phantom 4 digital camera (a) close to the plasma guns and (b) farther from the plasma guns. Contour plots of the camera eight-bit gray scale are shown before the external anode is switched on. Two radially localized axially extended channels for both axial locations are visible. The round features at the periphery are a result of the round vacuum viewport.

For the simplest magnetic reconnection experiment, the visible light emission from two current channels was monitored during their merging along the RSX axis. Two plasma guns with nozzles at $z=0$ cm spaced approximately 5.5 cm apart along a diameter were operated with basic discharge parameters $B_z=400$ G, $P_{\text{gas}}=20$ psi, and $V_{\text{bias}}=200$ V. The plasma discharge was initiated at $t=0$ and the external bias voltage was switched on at $t=1$ ms for a 2 ms period.

The visible light emission was monitored by a Phantom 4 fast framing camera⁴⁷ that viewed the two plasma channels perpendicularly from the top of the RSX vessel. Figures 8 and 9 show contour plots of the camera eight-bit gray scale frames (a) for $V_{\text{bias}}=0$ and 200 V, respectively. The frames in Figs. 8(a) and 9(a) were taken near the plasma guns at the axial location, $z \approx 15$ cm. The frames in Figs. 8(b) and 9(b) were taken farther from the plasma guns at the axial location, $z \approx 50$ cm. The round features at the periphery are a result of the round vacuum viewport. Some reflections near the edges are due to our less than ideal viewing dump. The camera exposure time and frame to frame time interval were, respectively, 117 and 270 μs . The Phantom 4 camera was free running and the data acquisition stop trigger was synchronized to initiation of the arc trigger, thus the reference time for each frame has an actual uncertainty of half the framing time or 135 μs . In order to resolve unambiguously the visible light emission before and after the bias is turned on, the

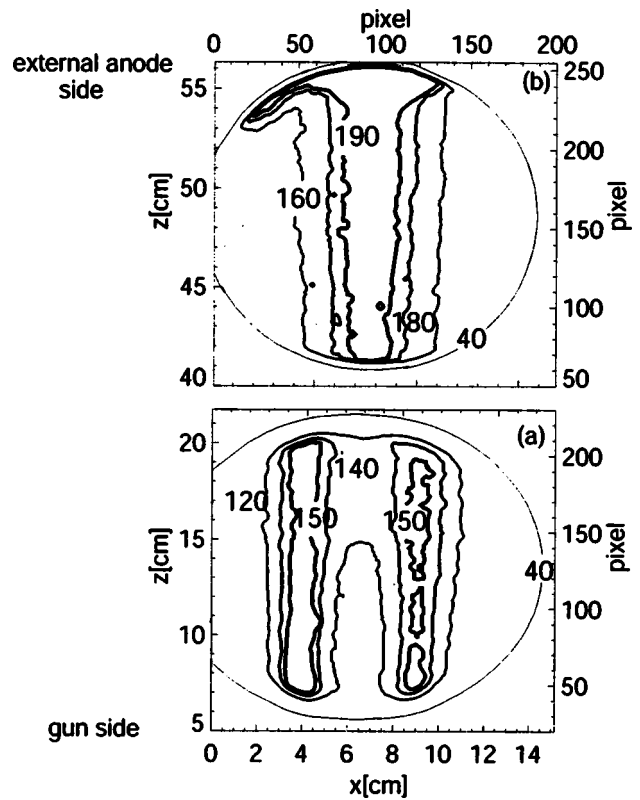


FIG. 9. Visible light emission measured by a Phantom 4 digital camera (a) close to the plasma guns and (b) farther from the plasma guns. Contour plots of the camera eight-bit gray scale are shown after the external anode is switched on. Two radially localized axially extended structures are visible at $z \approx 15$ cm. A single compact structure is visible at $z \approx 50$ cm, suggesting merging of the two current channels along the RSX axis.

frames in Figs. 8 and 9 correspond to nominal time of 810 and 1350 μs .

Before V_{bias} is switched on, the visible emission shows two radially localized and axially extended channels for both axial locations with no apparent spreading of the emission profile, Fig. 8. After the bias is switched on, the visible light structures remain distinct near the plasma guns, Fig. 9(a), but have merged into one axially extended radially compact structure at $z \approx 50$ cm, Fig. 9(b). We interpret this behavior as the signature of two current channels merging along the RSX axis. The time evolution of the visible light emission during merging cannot be resolved with the present camera framing speed and shutter gate times.

The visible light emission is mostly red, consistent with H_α Balmer emission from excited neutral hydrogen permeating each plasma channel. For plasma conditions not too different from these in the present experiment, Fiksel⁴² showed that hydrogen Balmer emission, neutral density, and plasma density profiles are approximately similar, therefore the visible emission in Figs. 8 and 9 can crudely indicate the plasma density structure of each channel, as suggested by Fig. 9(b). The visible emission contours are also consistent with current profile measurements.⁵² Each current channel has a radial distribution 15 cm downstream of the gun nozzle, similar to the current density profile shown in Fig. 6 for $V_{\text{bias}}=200$ V. In the nozzle area in front of the gun the entire current density must be radially localized to the 1 cm

TABLE I. Comparison of parameters of existing magnetic reconnection experiments.

Parameter	Unit	LAPD	TS-3	MRX	SSX	VTF	RSX
S		1–10	200	800	300	1000	<800
$r_{Gi} = c_s / \omega_{ci}$	cm	40	0.5	0.5	0.5	3	0.1–4
$\delta_e = c / \omega_{pe}$	mm	6	0.3–0.6	0.3–0.6	0.3–6	5.3	0.3–2
$\delta_i = c / \omega_{pi}$	cm	24	1–2	1–2	2	23	1–7

diameter aperture and is presumably very large. By the time the current channels have propagated as far as $z \approx 42$ cm, they have merged into one single current channel. In the axial region $15 \text{ cm} \leq z \leq 42 \text{ cm}$, the magnetic topology must change from double distinct sets of nested flux surfaces to one merged set. In future work we intend to experimentally investigate this region.

IV. DISCUSSION

The design and construction of the RSX device at Los Alamos National Laboratory was presented. The RSX is suitable for the study of three-dimensional magnetic reconnection during the coalescence of parallel current channels. The RSX takes advantage of recently developed plasma gun technology to create hydrogen plasma current channels of high current density ($J \leq 1 \text{ MA/m}^2$), resulting in electron densities and temperatures in the range of $n_e \approx 1\text{--}30 \times 10^{13} \text{ cm}^{-3}$ and $T_e \approx 10\text{--}20 \text{ eV}$. One major advantage of plasma gun technology is that it allows a high degree of flexibility in scaling independently the different parameters important in the reconnection process. The ranges of adjustable experimental parameters are appropriate for the study of magnetic reconnection in both collisional and collisionless regimes ($S < 800$). RSX plasmas are pulsed ($\approx 10 \text{ ms}$ duration) and thus compatible with internal probes as well as with noninvasive optical diagnostics. The reproducibility of the plasma conditions with small shot to shot variation shown in Fig. 5 leads to optimism that 3D measurements of the plasma dynamics will be as meaningful as the pioneering work of Gekelman *et al.*^{30,48} Table I shows a comparison of RSX parameters to existing magnetic reconnection experiments.

There are significant differences between a linear experiment such as RSX and other experiments in which magnetic reconnection is studied either in toroidal cusp geometry⁴¹ or by merging toroidal bundles of plasmas.^{32,35,40} Whereas toroidal systems are not affected by end effects that might obscure interpretation of the experimental results, it may be an issue in linear systems. Previous linear EMHD experiments at the University of California, at Los Angeles (UCLA)^{30,31} did not appear to suffer end effects due to possible line tying of field lines terminating on the end anode. For an estimate of the order of magnitude of these effects on the RSX, we will assume a nominal Spitzer resistivity of $5 \mu\Omega \text{ m}$ for an electron temperature of $T_e \approx 15 \text{ eV}$. This includes a factor of 2 conductivity enhancement from the drifting electron population.⁵³ The electric field required to support $0.5\text{--}1 \text{ MA/m}^2$ is approximately $2\text{--}5 \text{ V/m}$, leading due to a voltage drop of $8\text{--}20 \text{ V}$ along the 4 m column, which is on the order of T_e/e . If the ends are line tied by perfectly conducting end

boundaries, all radial and azimuthal electric fields would be shorted out to zero. On the other hand, local parallel voltage drops due to increased resistivity are likely also be of the order of T_e/e . Because of axial insulation, the plasma could support nonuniform local axial, radial, or azimuthal electric field profiles. These resistivity effects could follow from turbulence, including wave–wave, wave–particle scattering, and reconnection mechanisms.

Another important issue is to estimate the effects of electron–neutral collisions that might interfere with the collective plasma physics we are trying to observe. The plasma downstream of the gun is typically 30%–80% ionized depending on the discharge parameters. The plasma column close to the gun nozzle is nearly completely ionized⁵⁴ and the plasma density is comparable to or larger than the surrounding neutral density. The total gas load emitted from the gun can be estimated from the rise in neutral pressure determined with a Bayard–Alpert ion gauge to $5 \times 10^{-4} \text{ Torr}$ after a discharge. For the set of discharges in Fig. 7, this corresponds to a neutral density of $n_{\text{H}_2} \approx 1.7 \times 10^{13} \text{ cm}^{-3}$ for H_2 which is approximately 50% of the typical plasma density of $3.5 \times 10^5 \text{ cm}^{-3}$ shown in Fig. 7. The vessel volume is $5.5 \times 10^5 \text{ cm}^{-3}$, so the particle inventory for this maximum neutral pressure corresponds to approximately $8 \times 10^{18} \text{ H}_2$ molecules.

The electron–ion collision time τ_{ei} is approximately $8\text{--}80 \text{ ns}$ for electron temperatures in the range of $4\text{--}20 \text{ eV}$. In this range, the total reaction rate for electrons on diatomic hydrogen is $\langle \sigma v \rangle \approx 1.2 \times 10^{-7} \text{ cm}^3/\text{s}$.⁵⁵ Atomic hydrogen also exists, and the reaction rate for electrons is much smaller for electron temperatures of interest. For a neutral density of $n_{\text{H}_2} \approx 2 \times 10^{13} \text{ cm}^{-3}$, $\tau_{en} \approx 420 \text{ ns} \approx (7\text{--}70) \times \tau_{ei}$, indicating that electron–neutral collisions are a negligible effect. Collision rates with excited hydrogen neutrals can be two orders of magnitude larger but the density of excited atoms is likely to be small since they are quickly ionized.

The visible light emission contours shown in Figs. 8 and 9 are the RSX initial measurements during the coalescence of parallel current channels. The associated physics of magnetic reconnection processes will be the subject of future investigations with 3D measurements of magnetic structures and fluctuations.

ACKNOWLEDGMENTS

This work was supported by the Los Alamos Laboratory Directed Research and Development Exploratory Research program. The authors are grateful for the valuable assistance and support of R. Maqueda.

- ¹R. G. Giovanelli, *Nature (London)* **158**, 81 (1946).
- ²V. M. Vasyliunas, *Rev. Geophys. Space Phys.* **13**, 303 (1975).
- ³S. Tsuneta *et al.*, *Sol. Phys.* **136**, 37 (1991).
- ⁴R. M. Kulsrud, *Phys. Plasmas* **2**, 1735 (1995).
- ⁵Y. Shi, C. C. Wu, and L. C. Lee, *Geophys. Res. Lett.* **15**, 295 (1988).
- ⁶Y. Saito *et al.*, *J. Geophys. Res.* **100**, 567 (1995).
- ⁷M. Oieroset *et al.*, *Nature (London)* **412**, 414 (2001).
- ⁸S. A. Colgate *et al.*, *Phys. Plasmas* **8**, 2425 (2001).
- ⁹B. B. Kadomtsev, *Sov. J. Plasma Phys.* **1**, 389 (1976).
- ¹⁰S. Martini *et al.*, *Plasma Phys. Controlled Fusion* **41**, A315 (1999).
- ¹¹P. A. Sweet, *Electromagnetic Phenomena in Cosmical Physics*, edited by

- B. Lehnert (Cambridge University Press, New York, 1958).
- ¹²E. N. Parker, *J. Geophys. Res.* **62**, 509 (1957).
- ¹³E. N. Parker, *Astrophys. J.* **180**, 247 (1973).
- ¹⁴E. N. Parker, *Cosmical Magnetic Fields* (Clarendon, Oxford, 1979).
- ¹⁵A. Bhattacharjee *et al.*, *Phys. Plasmas* **8**, 1829 (2001).
- ¹⁶J. F. Drake *et al.*, *Bull. Am. Phys. Soc.* **46**, 144 (2001).
- ¹⁷J. Birn *et al.*, *J. Geophys. Res.* **106**, 3715 (2001).
- ¹⁸P. L. Pritchett, *J. Geophys. Res.* **106**, 25 (2001).
- ¹⁹G. Lapenta and J. Brackbill, *Bull. Am. Phys. Soc.* **46**, 331 (2001).
- ²⁰S. I. Syrovatsky, *Sov. Phys. Tech. Phys.* **18**, 580 (1973).
- ²¹N. Ohya, *Phys. Fluids* **17**, 2009 (1974).
- ²²A. G. Frank, *Plasma Physics and Electronics*, edited by L. M. Kovrizhnykh (Nova Science, Commack, NY, 1989).
- ²³A. G. Frank and S. Y. Bogdanov, *Earth, Planets Space* **53**, 531 (2001).
- ²⁴P. J. Baum and A. Bratenahl, *Adv. Electron. Electron Phys.* **54**, 1 (1980).
- ²⁵R. L. Stenzel and W. Gekelman, *J. Geophys. Res.* **88**, 4793 (1983).
- ²⁶W. Gekelman and R. L. Stenzel, *J. Geophys. Res.* **86**, 659 (1981).
- ²⁷W. Gekelman and R. L. Stenzel, *J. Geophys. Res.* **87**, 101 (1982).
- ²⁸W. Gekelman and R. L. Stenzel, *J. Geophys. Res.* **89**, 2715 (1984).
- ²⁹W. Gekelman and H. Pfister, *Phys. Fluids* **31**, 2017 (1988).
- ³⁰W. Gekelman, *Phys. Scr.*, T **12**, 277 (1982).
- ³¹W. Gekelman, *IEEE Trans. Plasma Sci.* **20**, 614 (1992).
- ³²M. Yamada *et al.*, *Phys. Rev. Lett.* **65**, 721 (1990).
- ³³Y. Ono *et al.*, *Phys. Fluids B* **5**, 3691 (1993).
- ³⁴Y. Ono *et al.*, *Phys. Rev. Lett.* **76**, 3328 (1996).
- ³⁵M. Yamada *et al.*, *Phys. Rev. Lett.* **78**, 3117 (1997).
- ³⁶H. Ji *et al.*, *Phys. Rev. Lett.* **80**, 3256 (1998).
- ³⁷M. R. Brown, *Phys. Plasmas* **6**, 1717 (1999).
- ³⁸M. R. Brown, *Phys. Plasmas* **9**, 2077 (2002).
- ³⁹T. W. Kornack *et al.*, *Phys. Rev. E* **58**, R36 (1998).
- ⁴⁰C. G. R. Geddes *et al.*, *Phys. Plasmas* **5**, 1027 (1998).
- ⁴¹J. Egedal *et al.*, *Rev. Sci. Instrum.* **71**, 3351 (2000).
- ⁴²G. Fiksel, Ph.D. thesis, University of Wisconsin–Madison, Madison, WI, 1991.
- ⁴³G. Fiksel *et al.*, *Plasma Sources Sci. Technol.* **5**, 78 (1996).
- ⁴⁴R. E. Siemon *et al.*, *Fusion Technol.* **9**, 13 (1986).
- ⁴⁵R. N. Dexter *et al.*, *Fusion Technol.* **19**, 131 (1991).
- ⁴⁶E. Torbert *et al.* (unpublished).
- ⁴⁷Photo-Sonics, Inc., 820 S. Mariposa Street, Burbank, CA 91506; <http://www.photosonics.com/>.
- ⁴⁸R. L. Stenzel *et al.*, *Geophys. Res. Lett.* **9**, 680 (1982).
- ⁴⁹G. Flor *et al.*, *Proceedings of the 16th Symposium on Fusion Technology*, London, 3–7 September, 1990, pp. 1272–1276.
- ⁵⁰X. Wang *et al.*, *J. Geophys. Res.* **27**, 633 (2000).
- ⁵¹R. Horiuchi and T. Sato, *Phys. Plasmas* **4**, 277 (1997).
- ⁵²T. Intrator *et al.* (unpublished).
- ⁵³J. D. Callen, Rep. No. UWPR 89-2, Dept. NEEP, University of Wisconsin–Madison, 1989, p. 516.
- ⁵⁴D. J. DenHartog *et al.*, *Plasma Sources Sci. Technol.* **6**, 492 (1997).
- ⁵⁵S. C. Brown, *Basic Data of Plasma Physics* (Chapman and Hall, London, 1959).